Letter

# Chemically Laminating Graphene Oxide Nanosheets with Phenolic Nanomeshes for Robust Membranes with Fast Desalination

Qianqian Lan, Chao Feng, Zicheng Wang, Le Li, Yong Wang,* and Tianxi Liu*

Read Online

ACCESS | Metrics & More | Article Recommendations | SI Supporting Information

**ABSTRACT:** Graphene oxide (GO) is receiving tremendous attention in membrane separation; however, its desalination performances remain suboptimal because of excessive swelling and tortuous transport pathways. Herein, we chemically joint GO nanosheets and phenolic nanomeshes together to form laminated membranes comprising through-plane nanopores and stabilized nanochannels. GO and phenolic/polyether nanosheets are mixed to form stacked structures and then treated in $H_2SO_4$ to remove polyether to produce nanomeshes and to chemically joint GO with phenolic nanomeshes. Thus-synthesized laminated membranes possess enhanced interlayer interactions and narrowed interlayer spacings down to 6.4 Å. They exhibit water permeance up to 165.6 L/(m² h bar) and $Na_2SO_4$ rejection of 97%, outperforming most GO-based membranes reported so far. Moreover, the membranes are exceptionally stable in water because the chemically jointed laminates suppress the swelling of GO. This work reports hybrid laminated structures of GO and phenolic nanomeshes, which are highly desired in desalination and other applications.

**KEYWORDS:** graphene oxide, phenolic nanomesh, membrane, chemical laminating, desalination
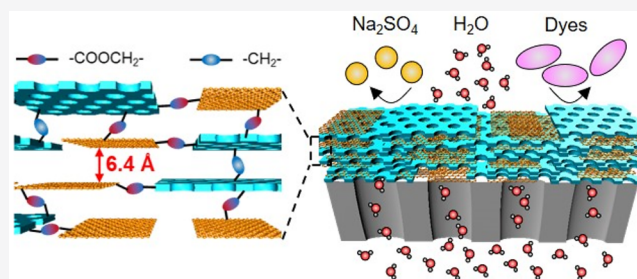
Graphene oxide (GO), holding the merits of atomic thickness, versatile surface functionalities, and good mechanical stability, has received extensive attention as a building block in the preparation of next-generation membranes.[1,2] The abundant oxygenated groups endow GO with good solution processability, facilitating the construction of ultrathin and robust laminated GO membranes.[3] Simulations and experiments have demonstrated the ultrafast and selective water/ion separation performances of laminated GO membranes.[4] The interlayer nanochannels confined by stacked GO afford exceptional transport behaviors.[5] The fast water transport is enabled by the unique nanocapillary network within the nanochannels originated from pristine $sp^2$ carbon regions of GO, in which water molecules exhibit large slip lengths and low frictional flow.[6,7] Meanwhile, pristine $sp^2$ carbon regions and oxidized regions of GO provide diverse interplays between nanochannel walls and ions such as cation-$\pi$ and electrostatic interactions, enabling highly selective ion transport.[8,9] Moreover, the confined nanochannels functioning as selective sieves can physically exclude ions with sizes larger than the subnanometer interlayer spacings.[10] Therefore, precise regulation in chemistry and microstructures of laminated GO membranes is always pursued to realize fast and efficient desalination.[11,12]

However, several issues hinder further progress and practical desalination applications of GO membranes. The unfavorable swelling effect due to excessive intercalation of water molecules into the nanochannels tends to enlarge the interlayer spacings, which disintegrates the laminar GO structures and deteriorates the selective exclusion of ions.[13] Enhancing interactions between stacked GO by reducing/modifying oxygenated moieties and cross-linking may engineer stabilized nanochannels with tailored chemistry for selective ion exclusion;[14,15] however, the water transport is inevitably compromised, which is known as the trade-off effect between permeability and selectivity.[16] Therefore, there remains a high demand for effective approaches to realize fast water transport while retaining ion exclusion through stable GO nanochannels.

To address the above issues, introducing through-plane nanoporous nanosheets in GO membranes that simultaneously enhances interlayer interactions emerges as the effective strategy. The nanoporous nanosheets with customized chemistry can uniformly and strongly interact with GO by exerting large basal planes, which are superior to the single-site interaction between molecular/ionic modifiers or cross-linkers and GO planes. Moreover, their similar two-dimensional (2D) structures guarantee the well-defined laminated microstruc-
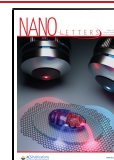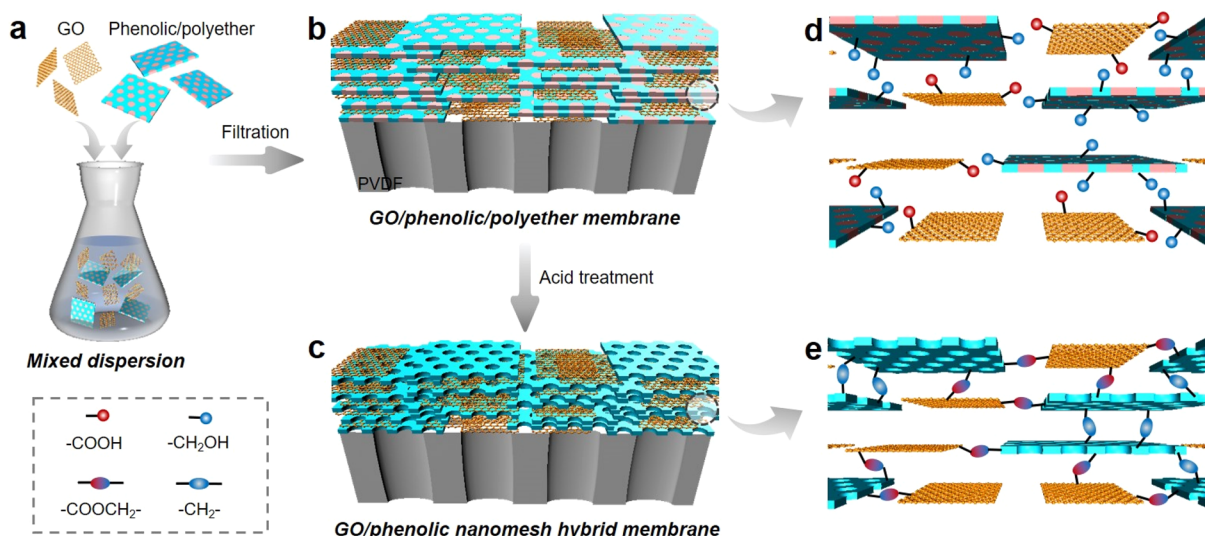
**Figure 1.** Schematic illustration for the preparation of GO/phenolic nanomesh hybrid membranes.
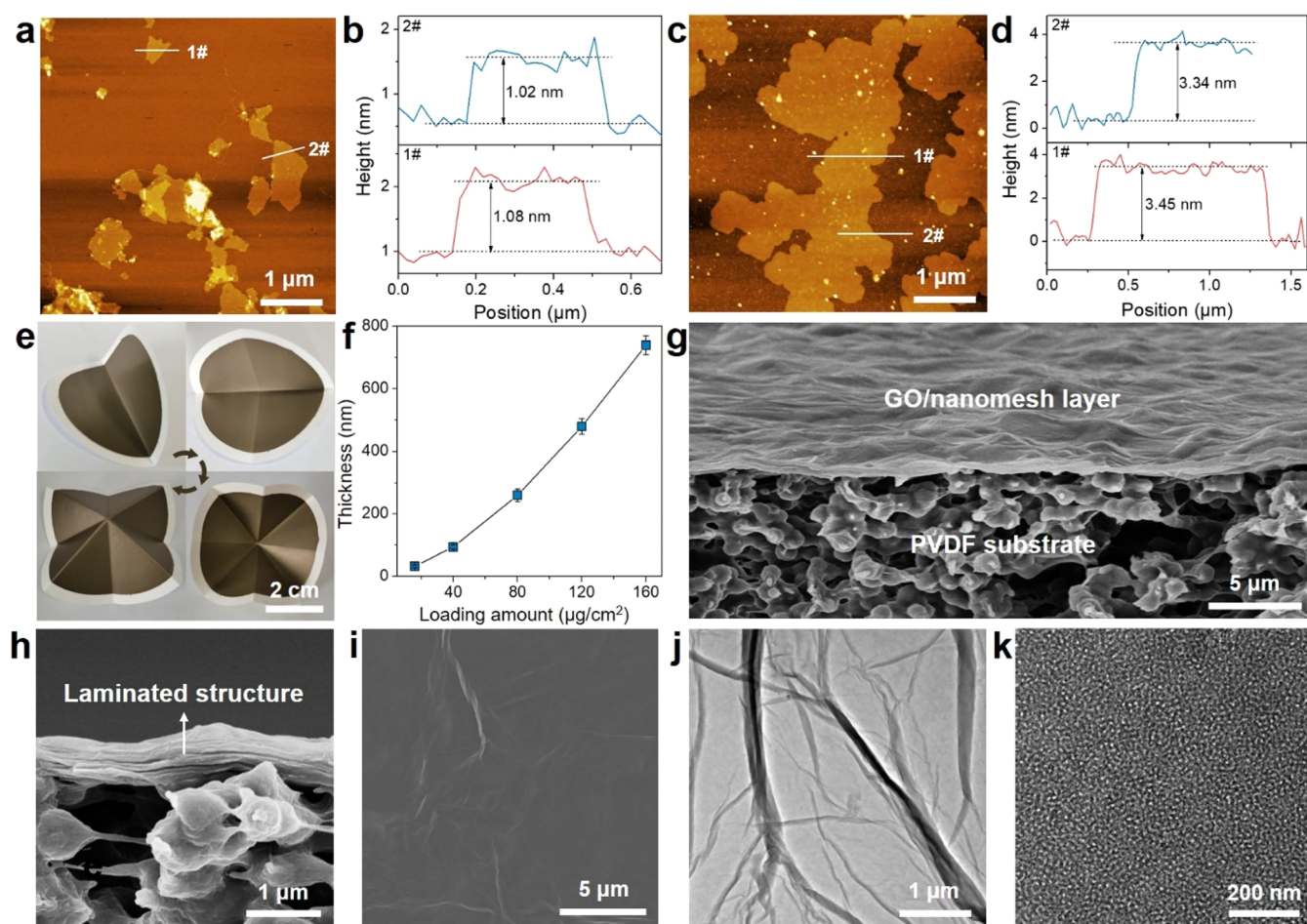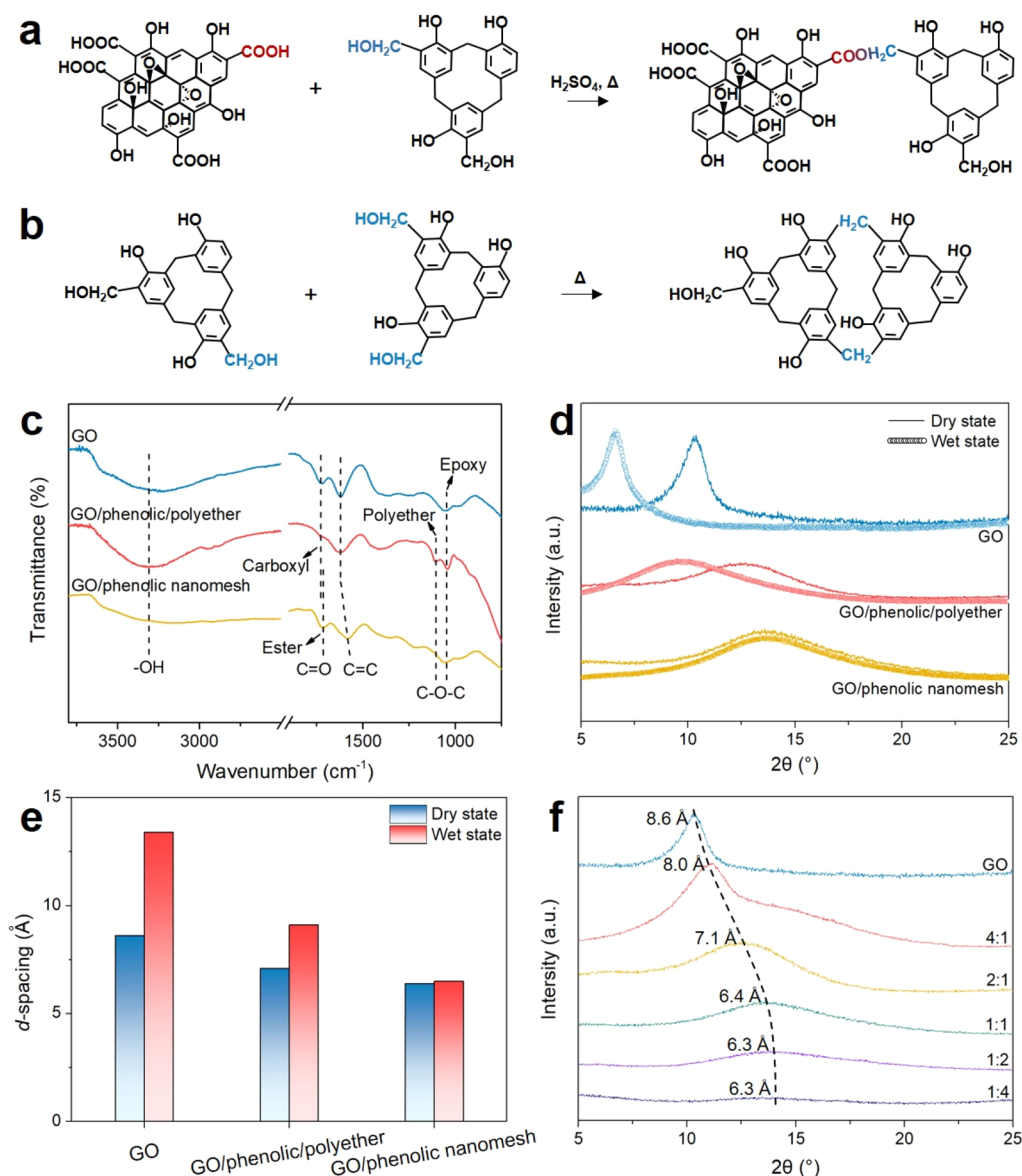


**Figure 2.** Morphologies of GO/phenolic nanomesh hybrid membranes. (a) AFM image and (b) corresponding height profiles of GO nanosheets. (c) AFM image and (d) corresponding height profiles of phenolic nanomeshes. (e) Photographs of the 1:1 hybrid membranes fabricated at the loading amount of 80 $\mu g/cm^2$ after several folds. (f) Relationship between the loading amounts of GO/phenolic/polyether nanosheets and the thicknesses of the 1:1 hybrid membranes. (g, h) Cross-sectional and (i) surface SEM images of the 1:1 hybrid membrane fabricated at the loading amount of 160 $\mu g/cm^2$. (j, k) TEM images of the 1:1 hybrid membrane prepared at the loading amount of 8 $\mu g/cm^2$.

tures of membranes, maintaining the nanochannels confined by adjacent nanosheets and ensuring precise sieving performances. More importantly, the through-plane nanoporous nanosheets can provide numerous vertically aligned pores, creating extra pathways and shorter distances to enable faster water transport. To this end, drilling pores on pristine

**Figure 3.** Physicochemical properties of GO/phenolic nanomesh hybrid membranes. Chemical reactions of (a) esterification between GO and phenolic nanomesh and (b) methylene linkage between neighboring phenolic nanomeshes. (c) FTIR spectra. (d) XRD patterns and (e) *d*-spacing values of pure GO membrane and the 1:1 hybrid membrane before and after acid treatment. (f) XRD patterns and *d*-spacing values of hybrid membranes with varied proportions.

nonporous GO by irradiation, chemical etching, and reduction/combustion methods has been proposed as the most straightforward approach.[17,18] However, precise control on pore size/position distributions is difficult, and defects are inevitably formed, leading to sacrificed selectivity.[19] Alternatively, researchers stacked GO with intrinsic nanoporous nanosheets such as metal−organic frameworks (MOFs)[20,21] and covalent organic frameworks (COFs).[22−24] However, this effort was hindered by insufficient interlayer interactions and inferior chemical stabilities of these framework nanosheets. Consequently, the water permeance of thus-prepared membranes was much lower than expected, and only 5% of salt ions can be excluded. Therefore, developing porous nanosheets that strongly interacted with GO and laminating them for membranes with high-efficient ion exclusion while retaining fast water transport are highly demanded, but remain challenging.

Inspired by ordered through-plane nanopores, ultrathin thicknesses, rich functional groups, and excellent chemical and mechanical robustness of 2D nanoporous phenolics[25,26] (known as phenolic nanomeshes), we foresee that they may become a potential candidate to adjust interlayer interaction, porous nature, and consequently transport behavior of stacked GO. Indeed, phenolic nanomeshes have been reported to interact with GO by strong noncovalent forces including hydrogen-bonds, amphiphilic interactions, and π−π interactions.[27,28] Herein, we explore the possibility of phenolic nanomeshes in tuning microstructure and interlayer chemistry of stacked GO, and prepare GO/phenolic nanomesh hybrid membranes with adjustable nanochannels for precise ion exclusion and fast water transport. The hybrid membranes are prepared by vacuum filtrating mixed dispersions of GO and phenolic/polyether nanosheets (precursor of phenolic nanomeshes) on macroporous substrates, followed by soaking in

$H_2SO_4$ (Figure 1a−c). Acid treatment can remove polyethers to generate through-plane nanopores and chemically joint GO and phenolic nanomeshes together (Figure 1d−e). Such a chemically jointed hybrid structure tightens and stabilizes the GO nanochannels and suppresses the swelling of GO in water. Benefiting from short through-plane pathways across phenolic nanomeshes, tightened nanochannels, and chemically jointed structures, thus-synthesized membranes realize fast and selective water/ion separations and exhibit superior stability for desalination.

**Results and Discussion.** GO was prepared by the modified Hummer's method, and phenolic/polyether nanosheets were synthesized via a glycerol-triggered 2D assembly strategy.[26,29] GO nanosheets are in the well-defined 2D morphology with lateral sizes of 0.3−1 $\mu$m (Figure 2a). The thickness of GO is ∼1 nm (Figure 2b). The $I_D/I_G$ value of GO is 0.81 (Figure S1). Phenolic/polyether nanosheets were treated in $H_2SO_4$ to remove polyethers, thus forming phenolic nanomeshes[30] with a uniform thickness of ∼3.4 nm, a through-plane pore size of ∼9.5 nm, and a lateral dimension of 2.5−5 $\mu$m (Figure 2c,d and Figure S2). Simply by filtrating mixed dispersions of GO and phenolic/polyether nanosheets on macroporous PVDF substrates followed by acid treatment, the GO/phenolic nanomesh hybrid membranes were obtained. We first mixed the dispersions of GO and phenolic/polyether nanosheets at the mass ratio of 1:1 to prepare hybrid membranes. The hybrid membrane maintains integrated without detachment after several folds due to the strong noncovalent interactions between the deposited GO/phenolic nanomesh layer and the substrate,[31] demonstrating the excellent flexibility and robustness of the membrane (Figure 2e). By changing the loading amounts of GO/phenolic/polyether nanosheets from 16 to 160 $\mu$g/cm$^2$, the hybrid membranes with darker colors and increased thicknesses from 33 to 740 nm can be easily prepared (Figure 2f and Figure S3). The cross-sectional SEM image reveals a continuous and uniform GO/phenolic nanomesh layer tightly attached to the surface of the PVDF substrate (Figure 2g). The GO/phenolic nanomesh layer exhibits a well-laminated structure because of the 2D natures of GO and phenolic nanomeshes (Figure 2h). Wrinkled structures can be observed on the surface of the hybrid membrane (Figure 2i) because of the good flexibility of nanosheets, the interactions between hydrophilic groups of nanosheets, and the drained water under nanosheets.[32] To investigate the through-plane nanopores of phenolic nanomeshes in the hybrid membranes, we prepared an ultrathin hybrid membrane with a thickness of ∼15 nm, and examined its morphology under TEM. The membrane possesses large numbers of wrinkles (Figure 2j), which agrees with the SEM observation. Uniform nanopores of phenolic nanomeshes can be recognized in the ultrathin hybrid membrane (Figure 2k). We then prepared hybrid membranes at varied mass ratios of GO and phenolic/polyether nanosheets. All membranes exhibit similar wrinkled surface morphologies and laminated cross-sectional structures (Figures S4 and S5). Their thicknesses are 250−290 nm when the loading amount is 80 $\mu$g/cm$^2$. We also prepared pure phenolic nanomesh membranes with a thickness of ∼250 nm, in which high-density through-plane nanopores can be clearly observed (Figure S6).

GO and phenolic nanomeshes can interact by strong noncovalent forces including hydrogen bonds, amphiphilic interactions, and $\pi−\pi$ interactions.[27,28] Importantly, $H_2SO_4$ treatment can induce chemical reactions between GO and phenolic nanomeshes (Figure 3a,b). The carboxyl groups of GO can react with the hydroxyl groups of phenolic nanomeshes to form ester groups.[33,34] Moreover, neighboring phenolic nanomeshes can join together by forming methylene bridges between benzene rings.[35] Therefore, the ester-bonded GO-phenolic nanomesh and methylene-bonded phenolic nanomesh-phenolic nanomesh lead to a covalently jointed structure of the hybrid membranes, in which GO nanosheets are *in situ* stabilized.

To reveal the physicochemical properties of the hybrid membranes, we first characterized the changes of chemical compositions of the 1:1 hybrid membrane before and after acid treatment (Figure 3c). Pure GO membrane shows characteristic peaks at 3320, 1725, 1615, and 1054 cm$^{-1}$, corresponding to the stretching vibrations of —OH, carboxylic C=O, aromatic C=C, and epoxy C—O—C, respectively.[36,37] These peaks remain unchanged after acid treatment, indicating the good chemical stability of GO (Figure S7). In the spectrum of the hybrid membrane before acid treatment, the peak at 1100 cm$^{-1}$ is ascribed to the stretching vibration of polyether C—O—C.[38] This peak disappears after acid treatment, implying that polyethers are removed. Moreover, the hybrid membrane after acid treatment exhibits a shifted peak at 1706 cm$^{-1}$ originated from the ester C=O, verifying the formation of ester groups.[39] The peak of C=C is shifted to 1579 cm$^{-1}$ due to the jointing of GO and phenolic nanomeshes via esterification.[40] In addition, the peak of —OH centered at 3320 cm$^{-1}$ is weakened after acid treatment due to the consumption of —OH in the formation of ester and methylene groups.[41] These results demonstrate that polyethers are removed and the hybrid membranes are chemically jointed during acid treatment. Such reactions are also confirmed by the change in membrane hydrophilicity (Figure S8).

Furthermore, we performed XRD analysis to investigate the interlayer spacings of the hybrid membranes (Figure 3d,e). In the dry state, the pure GO membrane exhibits a peak at 10.3° corresponding to a *d*-spacing of 8.6 Å. In the case of the 1:1 hybrid membrane before acid treatment, a peak at 12.5° corresponding to a decreased *d*-spacing of 7.1 Å is observed. After acid treatment, the peak is shifted to 13.8°, indicating a reduced *d*-spacing of 6.4 Å. Peaks of hybrid membranes are broader and weaker than that of the GO membrane, implying the poorer crystallite structure attributed to the partial replacement of GO with phenolic nanomeshes.[42] Notably, the *d*-spacing of pure GO membrane is almost unchanged after acid treatment, and pure phenolic nanomesh membrane exhibits no peak in the range of 5−25° (Figure S9). Therefore, the shifted peaks and suppressed *d*-spacings should be attributed to the interactions between the two types of nanosheets. In the hybrid membranes, the insertion of phenolic nanomeshes with a large lateral size leads to the few-layered GO laminates (Figure S10). Before acid treatment, the few-layered GO laminates are physically compressed by the noncovalent bonded nanosheets, leading to the slightly reduced interlayer spacing of GO. After acid treatment, the junction of phenolic nanomeshes by methylene linkages forms a cross-linked structure to provide tighter compression to the few-layered GO laminates, and phenolic nanomeshes are ester-bonded with GO, contributing to further narrowed interlayer spacing. The jointed structure is expected to achieve enhanced antiswelling stability in an aqueous milieu.[16] Therefore, we then characterized the *d*-spacings of these membranes in the wet state (Figure 3d,e). When membranes are immersed in
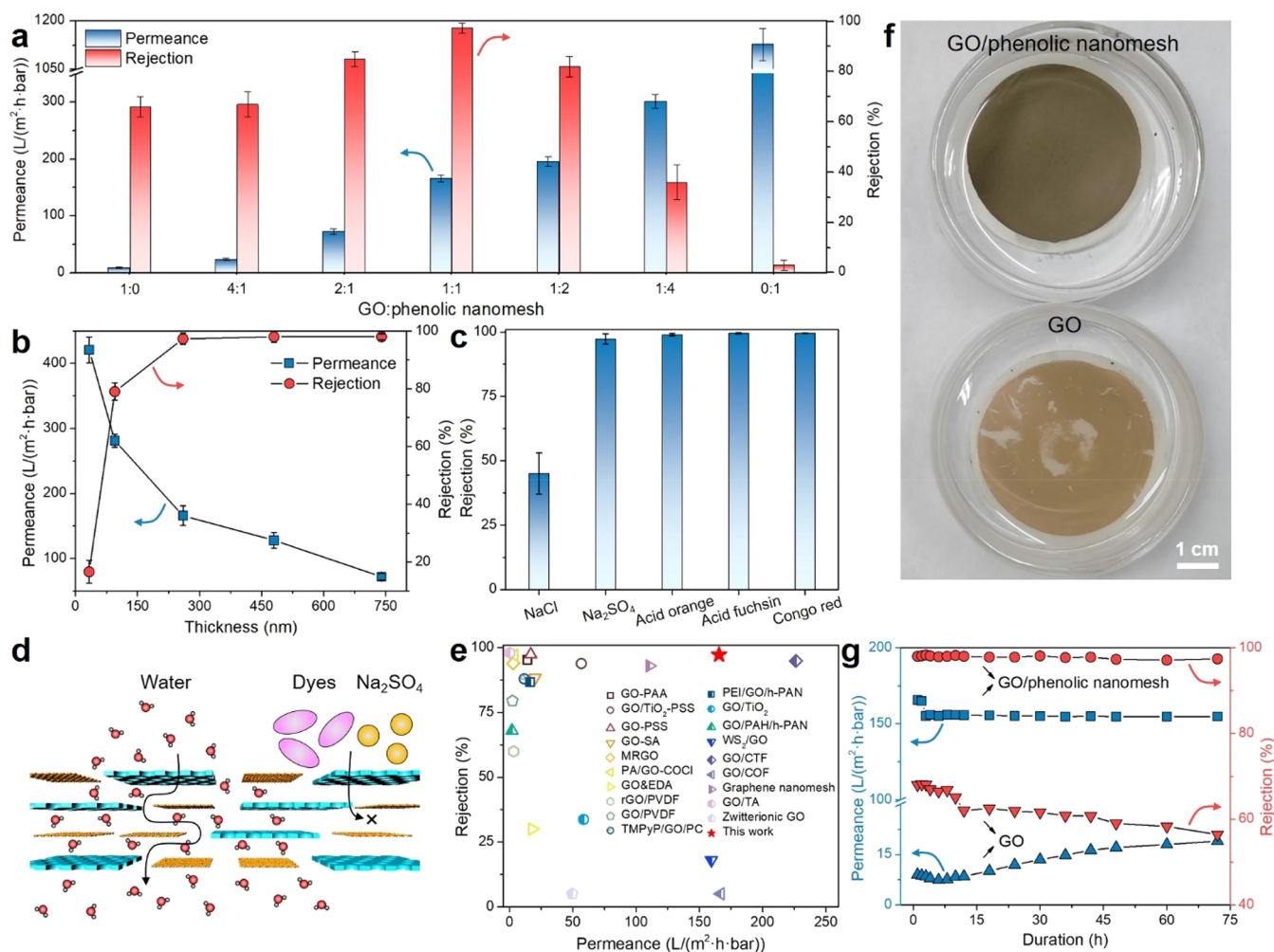
**Figure 4.** Separation performances of GO/phenolic nanomesh hybrid membranes. (a) Permeances and rejections to $Na_2SO_4$ of the hybrid membranes with varied proportions. (b) Permeances and rejections to $Na_2SO_4$ of the 1:1 hybrid membranes with varied thicknesses. (c) Rejections to different solutes of the 1:1 hybrid membrane with a thickness of 260 nm. (d) Schematic illustration of selective transport properties of the hybrid membranes. (e) Comparison of separation performances of the hybrid membranes with other reported membranes. (f) Photographs of the 1:1 hybrid membrane and pure GO membrane treated with sonication at 300 W for 10 min. (g) Permeances and rejections to $Na_2SO_4$ of the 1:1 hybrid membrane and pure GO membrane under long-term operations.

water for 24 h, the *d*-spacing of pure GO membrane is enlarged to 13.4 Å because of the excessive intercalation of water molecules. For the hybrid membrane before acid treatment, the *d*-spacing is mildly swelled to 9.1 Å. In particular, the hybrid membrane after acid treatment exhibits an almost unchanged *d*-spacing of 6.5 Å. Moreover, when the immersion duration is prolonged to 120 h, the *d*-spacing of the pure GO membrane is enlarged by 79.4% whereas that of the hybrid membrane is only 17.2% (Figure S11). These results testify that the hybrid membranes are structurally stable in water mainly due to the chemical joint effect. Moreover, with the increasing proportion of phenolic nanomeshes, the *d*-spacings are gradually decreased and the peaks become broader and weaker, suggesting that phenolic nanomeshes with higher contents lead to a stronger jointing effect on GO (Figure 3f).

Benefiting from the shortened through-plane pathways of phenolic nanomeshes and the suppressed GO nanochannels, the hybrid membranes are expected to enable fast and precise water/ion transport. We first measured water permeances and rejection properties of the hybrid membranes with varied mass ratios of GO and phenolic nanomeshes prepared at the loading amount of 80 $\mu g/cm^2$ (Figure 4a). The permeance of pure GO membrane is 9 L/($m^2$ h bar), which is increased to 24 L/($m^2$ h bar) for the 4:1 hybrid membrane. With the GO/phenolic nanomesh mass ratios increased to 2:1, 1:1, 1:2, and 1:4, the permeances of the hybrid membranes are increased to 73, 165, 196, and 301 L/($m^2$ h bar), respectively. Moreover, the rejection to $Na_2SO_4$ is 66% for pure GO membrane and is increased to 97% for the 1:1 hybrid membrane. When the mass ratios are further increased, the hybrid membranes exhibit decreased rejections. In addition, pure phenolic nanomesh membrane exhibits a permeance of 1128 L/($m^2$ h bar) and low rejection of 3%. In pure GO membrane, the GO nanochannels for water transport are long and tortuous, leading to low water permeances (Figure S12a). Phenolic nanomeshes possessing high-density nanopores provide plenty of pathways with shortened lengths for fast water transport (Figure S12b). Therefore, with the increasing proportions of phenolic nanomeshes, the hybrid membranes exhibit abundant shortened transport pathways and thus increased water permeances (Figure S12c,d). Meanwhile, the hybrid membrane is negatively charged (Figure S13), and the selective nanochannels between stacked GO are narrowed with the increased proportions of phenolic nanomeshes. Both the

Donnan theory and the size discrimination lead to the increased rejections of hybrid membranes. However, excessive phenolic nanomeshes enable dominating through-plane pathways for ions to transport across the membranes, resulting in decreased rejections. Overall, the 1:1 hybrid membrane gives both high permeance and high rejection.

We further measured water permeances and rejection properties of the 1:1 hybrid membranes with varied thicknesses. The permeance shows a decreased tendency while the $Na_2SO_4$ rejection is increased with the increase in thicknesses (Figure 4b). For example, the permeance of the hybrid membrane with a thickness of 33 nm is 421.4 L/(m$^2$ h bar), which is gradually decreased to 281.1, 165.6, 127.8, and 71.8 L/(m$^2$ h bar) when the thickness is increased to 95, 260, 480, and 740 nm, respectively. The $Na_2SO_4$ rejection of the hybrid membrane with a thickness of 33 nm is 17%. When the thickness is increased to 260 nm, 97% of $Na_2SO_4$ can be rejected by the hybrid membrane. The hybrid membranes with higher thicknesses exhibit longer transport pathways, leading to higher mass transfer resistances and thus decreased permeances (Figure S14). However, the hybrid membranes with extremely thin thicknesses may lack sufficient GO nanochannels for selective transport, resulting in free penetration of ions across the membranes through the nanopores of phenolic nanomeshes.

Furthermore, we determined the rejections of the 1:1 hybrid membrane with a thickness of 260 nm to different solutes including salts and dyes (Figure 4c). The rejections to NaCl, $Na_2SO_4$, and negatively charged dyes (Figure S15) are 45%, 97%, and exceeding 99%, respectively. Because the hydrated diameters of salt ions and the molecular sizes of dyes (Tables S1 and S2) are larger than the $d$-spacing of the hybrid membrane (6.4 Å), high rejections are expected according to the size-sieving effect.[43] However, NaCl cannot be efficiently rejected by the hybrid membrane. According to the Donnan theory, $Na^+$ can be attracted by negatively charged membranes.[44] Consequently, $Na^+$ may dehydrate and permeate through the hybrid membrane accompanied by $Cl^-$ for balancing the charges, leading to the transport of NaCl across the membrane.[45] By contrast, multivalent $SO_4^{2-}$ and dye anions with larger sizes can be strongly repulsed by the hybrid membrane,[46] thus leading to high rejections to $Na_2SO_4$ and dyes. Therefore, the size-sieving effect and Donnan effect synergistically contribute to the selective rejections of $Na_2SO_4$ and dyes while water molecules with a diameter of 2.8 Å can freely penetrate through the hybrid membranes (Figure 4d). It is prospected that monovalent ion-exclusion membranes can be realized by further narrowing interlayer spacings and enhancing membrane charges.

We compared the separation performances of the hybrid membranes with other GO-based membranes reported in the literature in terms of water permeance and $Na_2SO_4$ rejection (Figure 4e and Table S3). The hybrid membrane prepared in this work exhibits over 10 times higher permeance than other membranes with similar rejections. Moreover, compared to membranes with similar permeances, the hybrid membrane shows 5−20 times higher rejections. This highlights the fast and selective water/ion transport of the hybrid membrane benefiting from the nanopores of phenolic nanomeshes and the suppressed GO nanochannels. Prospectively, higher performances can be achieved by manipulating the size, density, and geometry of nanopores in nanomeshes.

Thanks to the chemically jointed structures, the hybrid membranes are expected to have enhanced stability. To demonstrate this, the hybrid membrane and pure GO membrane were treated in water under sonication at 300 W for 10 min. The hybrid membrane maintains its structural integrity, while the pure GO membrane is seriously damaged, indicating the good robustness of the hybrid membrane (Figure 4f). We then investigated the long-term performances of the hybrid membrane and pure GO membrane (Figure 4g). Both membranes exhibit slightly decreased permeances in the initial stage due to the structural compaction under the operating pressure. Afterward, pure GO membrane exhibits increased permeances and decreased rejections due to the structural disassembly at a high stirring speed (Figure S16), whereas the hybrid membrane maintains stable, benefiting from the chemically jointed structure. Moreover, the hybrid membrane exhibits good mechanical stability at elevated operating pressures (Figure S17). Therefore, the hybrid membranes can stably deliver the function of fast and selective water/ion transport. Such a good stability provides a potential opportunity for the hybrid membranes to be applied in practical desalination applications. Moreover, because of the chemical robustness of phenolics and GO, the hybrid membranes are promising in applications involving strong acids and organics.

In conclusion, we report on the preparation of GO/phenolic nanomesh hybrid membranes with short through-plane pathways and tightened nanochannels via a chemical laminating strategy for high-efficient desalination. Presynthesized phenolic/polyether nanosheets are used as the precursor of phenolic nanomeshes and mixed with GO at varied proportions to construct GO/phenolic/polyether membranes by vacuum filtration. After acid treatment, GO/phenolic nanomesh hybrid membranes are produced, in which GO and phenolic nanomesh are ester-bonded and adjacent phenolic nanomeshes are methylene-bonded. Such a chemically jointed structure leads to tightened interlayer spacings down to 6.4 Å. The through-plane nanopores of phenolic nanomeshes provide rich and short pathways for fast water transport, and the tightened GO nanochannels can selectively restrain ion transport. The hybrid membranes thereby show a high water permeance up to 165.6 L/(m$^2$ h bar) and $Na_2SO_4$ rejection of 97%, which are superior to other GO-based membranes. Good performance stability is achieved using thus-prepared hybrid membranes. This work provides a simple strategy to introduce through-plane nanopores into GO membranes for fast desalination and demonstrates the chemical jointing effect in controlling interlayer spacings. Moreover, this strategy is expected to be used in the design of other 2D-material-based nanochannels with enhanced performances.

## ■ ASSOCIATED CONTENT

### ⓢ Supporting Information

The Supporting Information is available free of charge at https://pubs.acs.org/doi/10.1021/acs.nanolett.1c02683.

Experimental procedures; characterizations and morphologies of GO nanosheets, phenolic nanomeshes, and GO/phenolic nanomesh hybrid membranes; schematic illustrations of interlayer spacings and transport pathways of membranes; separation performances of membranes (PDF)

## ■ AUTHOR INFORMATION

### Corresponding Authors

**Yong Wang** − *State Key Laboratory of Materials-Oriented Chemical Engineering, College of Chemical Engineering, Nanjing Tech University, Nanjing, Jiangsu 211816, People's Republic of China*; Email: yongwang@njtech.edu.cn

**Tianxi Liu** − *The Key Laboratory of Synthetic and Biological Colloids, Ministry of Education, School of Chemical and Material Engineering, Jiangnan University, Wuxi, Jiangsu 214122, People's Republic of China*; Email: txliu@jiangnan.edu.cn

### Authors

**Qianqian Lan** − *The Key Laboratory of Synthetic and Biological Colloids, Ministry of Education, School of Chemical and Material Engineering, Jiangnan University, Wuxi, Jiangsu 214122, People's Republic of China*

**Chao Feng** − *The Key Laboratory of Synthetic and Biological Colloids, Ministry of Education, School of Chemical and Material Engineering, Jiangnan University, Wuxi, Jiangsu 214122, People's Republic of China*

**Zicheng Wang** − *The Key Laboratory of Synthetic and Biological Colloids, Ministry of Education, School of Chemical and Material Engineering, Jiangnan University, Wuxi, Jiangsu 214122, People's Republic of China*

**Le Li** − *The Key Laboratory of Synthetic and Biological Colloids, Ministry of Education, School of Chemical and Material Engineering, Jiangnan University, Wuxi, Jiangsu 214122, People's Republic of China*

Complete contact information is available at:
https://pubs.acs.org/10.1021/acs.nanolett.1c02683

### Author Contributions

The manuscript was written through contributions of all authors. All authors have given approval to the final version of the manuscript.

### Notes

The authors declare no competing financial interest.

## ■ REFERENCES

(1) Huang, H.; Shi, H.; Das, P.; Qin, J.; Li, Y.; Wang, X.; Su, F.; Wen, P.; Li, S.; Lu, P.; Liu, F.; Li, Y.; Zhang, Y.; Wang, Y.; Wu, Z.-S.; Cheng, H.-M. The chemistry and promising applications of graphene and porous graphene materials. *Adv. Funct. Mater.* **2020**, *30* (41), 1909035.

(2) Zhang, W. H.; Yin, M. J.; Zhao, Q.; Jin, C. G.; Wang, N.; Ji, S.; Ritt, C. L.; Elimelech, M.; An, Q. F. Graphene oxide membranes with stable porous structure for ultrafast water transport. *Nat. Nanotechnol.* **2021**, *16* (3), 337−343.

(3) Guan, K.; Jia, Y.; Lin, Y.; Wang, S.; Matsuyama, H. Chemically converted graphene nanosheets for the construction of ion-exclusion nanochannel membranes. *Nano Lett.* **2021**, *21* (8), 3495−3502.

(4) Sun, P.; Wang, K.; Zhu, H. Recent developments in graphene-based membranes: Structure, mass-transport mechanism and potential applications. *Adv. Mater.* **2016**, *28* (12), 2287−310.

(5) Sun, P.; Zhu, M.; Wang, K.; Zhong, M.; Wei, J.; Wu, D.; Xu, Z.; Zhu, H. Selective ion penetration of graphene oxide membranes. *ACS Nano* **2013**, *7* (1), 428−437.

(6) Joshi, R. K.; Carbone, P.; Wang, F. C.; Kravets, V. G.; Su, Y.; Grigorieva, I. V.; Wu, H. A.; Geim, A. K.; Nair, R. R. Precise and ultrafast molecular sieving through graphene oxide membranes. *Science* **2014**, *343*, 752−754.

(7) Xu, F.; Song, Y.; Wei, M.; Wang, Y. Water flow through interlayer channels of two-dimensional materials with various hydrophilicities. *J. Phys. Chem. C* **2018**, *122* (27), 15772−15779.

(8) Liu, G.; Jin, W.; Xu, N. Graphene-based membranes. *Chem. Soc. Rev.* **2015**, *44* (15), 5016−5030.

(9) Zhao, G.; Zhu, H. Cation-$\pi$ interactions in graphene-containing systems for water treatment and beyond. *Adv. Mater.* **2020**, *32* (22), 1905756.

(10) Zhang, W.; Shi, M.; Heng, Z.; Zhang, W.; Pan, B. Soft particles enable fast and selective water transport through graphene oxide membranes. *Nano Lett.* **2020**, *20* (10), 7327−7332.

(11) Wen, Q.; Jia, P.; Cao, L.; Li, J.; Quan, D.; Wang, L.; Zhang, Y.; Lu, D.; Jiang, L.; Guo, W. Electric-field-induced ionic sieving at planar graphene oxide heterojunctions for miniaturized water desalination. *Adv. Mater.* **2020**, *32* (16), 1903954.

(12) Zhang, M.; Zhao, P.; Li, P.; Ji, Y.; Liu, G.; Jin, W. Designing biomimic two-dimensional ionic transport channels for efficient ion sieving. *ACS Nano* **2021**, *15* (3), 5209−5220.

(13) Zheng, S.; Tu, Q.; Urban, J. J.; Li, S.; Mi, B. Swelling of graphene oxide membranes in aqueous solution: Characterization of interlayer spacing and insight into water transport mechanisms. *ACS Nano* **2017**, *11* (6), 6440−6450.

(14) Zhang, M.; Mao, Y.; Liu, G.; Liu, G.; Fan, Y.; Jin, W. Molecular bridges stabilize graphene oxide membranes in water. *Angew. Chem., Int. Ed.* **2020**, *59* (4), 1689−1695.

(15) Chen, L.; Shi, G.; Shen, J.; Peng, B.; Zhang, B.; Wang, Y.; Bian, F.; Wang, J.; Li, D.; Qian, Z.; Xu, G.; Liu, G.; Zeng, J.; Zhang, L.; Yang, Y.; Zhou, G.; Wu, M.; Jin, W.; Li, J.; Fang, H. Ion sieving in graphene oxide membranes via cationic control of interlayer spacing. *Nature* **2017**, *550* (7676), 380−383.

(16) Zhang, L.; Zhang, M.; Liu, G.; Jin, W.; Li, X. Fungal cell wall-graphene oxide microcomposite membrane for organic solvent nanofiltration. *Adv. Funct. Mater.* **2021**, *31*, 2100110.

(17) Yang, Y.; Yang, X.; Liang, L.; Gao, Y.; Cheng, H.; Li, X.; Zou, M.; Ma, R.; Yuan, Q.; Duan, X. Large-area graphene-nanomesh/carbon-nanotube hybrid membranes for ionic and molecular nanofiltration. *Science* **2019**, *364*, 1057−1062.

(18) Surwade, S. P.; Smirnov, S. N.; Vlassiouk, I. V.; Unocic, R. R.; Veith, G. M.; Dai, S.; Mahurin, S. M. Water desalination using nanoporous single-layer graphene. *Nat. Nanotechnol.* **2015**, *10* (5), 459−464.

(19) Su, P.; Wang, F.; Li, Z.; Tang, C. Y.; Li, W. Graphene oxide membranes: Controlling their transport pathways. *J. Mater. Chem. A* **2020**, *8* (31), 15319−15340.

(20) Rao, Z.; Feng, K.; Tang, B.; Wu, P. Surface decoration of amino-functionalized metal-organic framework/graphene oxide composite onto polydopamine-coated membrane substrate for highly efficient heavy metal removal. *ACS Appl. Mater. Interfaces* **2017**, *9* (3), 2594−2605.

(21) Li, W.; Zhang, Y.; Su, P.; Xu, Z.; Zhang, G.; Shen, C.; Meng, Q. Metal-organic framework channelled graphene composite membranes for $H_2/CO_2$ separation. *J. Mater. Chem. A* **2016**, *4* (48), 18747−18752.

(22) Sui, X.; Yuan, Z.; Liu, C.; Wei, L.; Xu, M.; Liu, F.; Montoya, A.; Goh, K.; Chen, Y. Graphene oxide laminates intercalated with 2D covalent-organic frameworks as a robust nanofiltration membrane. *J. Mater. Chem. A* **2020**, *8* (19), 9713−9725.

(23) Kong, G.; Pang, J.; Tang, Y.; Fan, L.; Sun, H.; Wang, R.; Feng, S.; Feng, Y.; Fan, W.; Kang, W.; Guo, H.; Kang, Z.; Sun, D. Efficient dye nanofiltration of a graphene oxide membrane via combination with a covalent organic framework by hot pressing. *J. Mater. Chem. A* **2019**, *7* (42), 24301−24310.

(24) Khan, N. A.; Yuan, J.; Wu, H.; Cao, L.; Zhang, R.; Liu, Y.; Li, L.; Rahman, A. U.; Kasher, R.; Jiang, Z. Mixed nanosheet membranes assembled from chemically grafted graphene oxide and covalent organic frameworks for ultra-high water flux. *ACS Appl. Mater. Interfaces* **2019**, *11* (32), 28978−28986.

(25) Qiu, P.; Zhao, T.; Fang, Y.; Zhu, G.; Zhu, X.; Yang, J.; Li, X.; Jiang, W.; Wang, L.; Luo, W. Pushing the limit of ordered mesoporous materials via 2D self-assembly for energy conversion and storage. *Adv. Funct. Mater.* **2021**, *31* (7), 2007496.

(26) Lan, Q.; Zhang, Z.; Xu, F.; Wei, M.; Wang, Y. Nanomeshes with sub-10 nm pores by glycerol-triggered 2D assembly in liquid phases for fast and selective membranes. *Nano Lett.* **2021**, *21* (7), 3302−3309.

(27) Liu, R.; Wan, L.; Liu, S.; Pan, L.; Wu, D.; Zhao, D. An interface-induced co-assembly approach towards ordered mesoporous carbon/graphene aerogel for high-performance supercapacitors. *Adv. Funct. Mater.* **2015**, *25* (4), 526−533.

(28) Fang, Y.; Lv, Y.; Tang, J.; Wu, H.; Jia, D.; Feng, D.; Kong, B.; Wang, Y.; Elzatahry, A. A.; Al-Dahyan, D.; Zhang, Q.; Zheng, G.; Zhao, D. Growth of single-layered two-dimensional mesoporous polymer/carbon films by self-assembly of monomicelles at the interfaces of various substrates. *Angew. Chem., Int. Ed.* **2015**, *54* (29), 8425−8429.

(29) Pu, L.; Li, S.; Zhang, Y.; Zhu, H.; Fan, W.; Ma, P.; Dong, W.; Wang, Z.; Liu, T. Polyimide-based graphene composite foams with hierarchical impedance gradient for efficient electromagnetic absorption. *J. Mater. Chem. C* **2021**, *9* (6), 2086−2094.

(30) Lan, Q.; Yan, N.; Wang, Y. Tight ultrafiltration membranes of mesoporous phenolic resin filled in macroporous substrates. *J. Membr. Sci.* **2017**, *533*, 96−102.

(31) Lan, Q.; Wang, Z.; Wang, Y. Mesoporous phenolics filled in macroporous membranes for tunable tight-ultrafiltration. *Chem. Eng. Sci.* **2018**, *187*, 98−106.

(32) Wei, Y.; Zhang, Y.; Gao, X.; Yuan, Y.; Su, B.; Gao, C. Declining flux and narrowing nanochannels under wrinkles of compacted graphene oxide nanofiltration membranes. *Carbon* **2016**, *108*, 568−575.

(33) Painer, D.; Lux, S. Intramolecular catalysis in carboxylic acid esterification: Modeling of single- and multi-acid esterification. *Ind. Eng. Chem. Res.* **2019**, *58* (3), 1133−1141.

(34) Manabe, K.; Iimura, S.; Sun, X. M.; Kobayashi, S. Dehydration reactions in water. Bronsted acid-surfactant-combined catalyst for ester, ether, thioether, and dithioacetal formation in water. *J. Am. Chem. Soc.* **2002**, *124* (40), 11971−11978.

(35) Wang, J.; Chang, Z.; Ding, B.; Li, T.; Yang, G.; Pang, Z.; Nakato, T.; Eguchi, M.; Kang, Y. M.; Na, J.; Guan, B. Y.; Yamauchi, Y. Universal access to two-dimensional mesoporous heterostructures by micelle-directed interfacial assembly. *Angew. Chem., Int. Ed.* **2020**, *59* (44), 19570−19575.

(36) Zhang, M.; Guan, K.; Ji, Y.; Liu, G.; Jin, W.; Xu, N. Controllable ion transport by surface-charged graphene oxide membrane. *Nat. Commun.* **2019**, *10* (1), 1253.

(37) Zhang, Y.; Zhuang, Y.; Yin, R.; Han, L.; Shen, Y.; Zhang, Z.; Xie, K.; Zhang, J.; Yuan, M.; Wang, J. A monolayer nanostructure based on polyhedral oligomeric silsesquioxane and graphene oxide for highly efficient separation of hemoglobin. *Compos. Commun.* **2021**, *25*, 100702.

(38) Lan, Q.; Yang, Y.; Guo, L.; Wang, Y. Gradient nanoporous phenolics filled in macroporous substrates for highly permeable ultrafiltration. *J. Membr. Sci.* **2019**, *576*, 123−130.

(39) Guo, L.; Jia, S.; Diercks, C. S.; Yang, X.; Alshmimri, S. A.; Yaghi, O. M. Amidation, esterification, and thioesterification of a carboxyl-functionalized covalent organic framework. *Angew. Chem., Int. Ed.* **2020**, *59*, 2023−2027.

(40) Huang, T.; Shao, Y. W.; Zhang, Q.; Deng, Y. F.; Liang, Z. X.; Guo, F. Z.; Li, P. C.; Wang, Y. Chitosan-cross-linked graphene oxide/ carboxymethyl cellulose aerogel globules with high structure stability in liquid and extremely high adsorption ability. *ACS Sustainable Chem. Eng.* **2019**, *7* (9), 8775−8788.

(41) Huo, X.; Lan, Q.; Wang, Y. In situ cavitation of phenolic supramolecules with PEO-PPO-PEO block copolymers by Friedel-Crafts alkylation toward ordered nanoporous polymers. *Ind. Eng. Chem. Res.* **2016**, *55* (22), 6398−6404.

(42) Qian, Y.; Shang, J.; Liu, D.; Yang, G.; Wang, X.; Chen, C.; Kou, L.; Lei, W. Enhanced ion sieving of graphene oxide membranes via surface amine functionalization. *J. Am. Chem. Soc.* **2021**, *143* (13), 5080−5090.

(43) Abraham, J.; Vasu, K. S.; Williams, C. D.; Gopinadhan, K.; Su, Y.; Cherian, C. T.; Dix, J.; Prestat, E.; Haigh, S. J.; Grigorieva, I. V.; Carbone, P.; Geim, A. K.; Nair, R. R. Tunable sieving of ions using graphene oxide membranes. *Nat. Nanotechnol.* **2017**, *12* (6), 546−550.

(44) Rajesh, S.; Bose, A. B. Development of graphene oxide framework membranes via the "from" and "to" cross-linking approach for ion-selective separations. *ACS Appl. Mater. Interfaces* **2019**, *11* (31), 27706−27716.

(45) Lv, Y.; Xia, J.; Yang, Y.; Chen, Y.; Liu, T. Thin-film composite membranes with mineralized nanofiber supports for highly efficient nanofiltration. *Compos. Commun.* **2021**, *24*, 100695.

(46) Wu, Y.; Fu, C. F.; Huang, Q.; Zhang, P.; Cui, P.; Ran, J.; Yang, J.; Xu, T. 2D heterostructured nanofluidic channels for enhanced desalination performance of graphene oxide membranes. *ACS Nano* **2021**, *15* (4), 7586−7595.